Progress In Electromagnetics Research C, Vol. 88, 13–25, 2018

A Semi-Analytical Approach for Fast Design of Microwave Metasheets with Circular Metal Rings on Dielectric Substrates

Ezgi Öziş[1, *], Andrey V. Osipov[1], and Thomas F. Eibert[2]

Abstract—Metasheets are ultra-thin sheets built from sub-wavelength resonators designed in order to achieve certain frequency-dependent transmission behaviour. A semi-analytical approach based on an equivalent circuit representation is proposed to calculate the microwave transmission through metasheets which consist of 2D periodic arrays of planar circular metal rings with and without substrate. The electromagnetic response of the metasheet can be controlled by changing the radius and periodicity of the circular rings. In the semi-analytical approach, the equations for impedances of the equivalent circuit are parameterized and fitted to match the values of transmission coefficients obtained by full-wave simulations at selected frequency points. Such an approach permits an optimization of the metasheet design with a very small number of full-wave numerical simulations. It is shown that the results of the semi-analytical approach match well with full-wave simulations and measurements within a reasonable range of radius and periodicity values.

1. INTRODUCTION

A radome may have a critical effect on the performance of radar systems and antennas, where signal phase and transmission uniformity are required to run the microwave system efficiently and properly [1]. For example, many antenna systems contain phased arrays which are utilized for beam scanning in transmit and receive operation. Direction finding (DF), scanning synthetic aperture radar (SAR) and similar applications mainly use such systems [2]. The radome can distort the phase of the signal leading to losses in DF accuracy and SAR resolution [2]. Metamaterials and metasheets can be used to control electromagnetic transmission in a desired way [3, 4]. The electromagnetic properties of metamaterials can be analyzed by using analytical and numerical methods. The analytical approaches include, for example, equivalent circuits, the transmission line approach [5, 6] as well as a combination of equivalence principle and impedance concepts [7–10]. The electromagnetic response of infinite periodic arrays can also be calculated by various numerical methods, see for example [11–13].

In numerical simulations of metasheets the main problems are long simulation times and heavy memory requirements. Due to the fine geometric details, metasheet unit-cells need a very fine meshing to achieve accurate results. The simulation time can be very long, especially when wide-band frequency responses are needed. Various numerical approaches for different electromagnetic applications, also combined with transmission-line modelling, have been developed to decrease the computational time and the memory requirements, increase the accuracy and simplify the simulation approaches [14–19]. An equivalent circuit approach is much faster, and it has been applied to periodic structures involving Jerusalem-crosses and square loops in [20, 21].

In this study periodic arrays of circular ring resonators and the effect of dielectric substrates are considered. The circular ring is a well-known building element of metasheets [22]. The major properties

Received 4 July 2018, Accepted 21 September 2018, Scheduled 31 October 2018

* Corresponding author: Ezgi Öziş (ezgi.oezis@dlr.de).

[1] Microwaves and Radar Institute, German Aerospace Center (DLR), Oberpfaffenhofen, Germany. [2] Chair of High-Frequency Engineering, Department of Electrical and Computer Engineering, Technical University of Munich, Germany.

of circular rings are that they are easy to manufacture and their response is independent of polarization. In contrast to similar particles, like the split ring resonator [23], there are no analytical expressions available for calculating its resonance frequency as a function of its geometrical parameters. We aim to determine the transmission in terms of the dimensions of the planar rings and the array periodicity (unit-cell size) for a plane wave incident normal to the metasheet at a microwave frequency. The transmission coefficient of an array structure can be defined in terms of an equivalent impedance, which depends on the radius of the rings and the periodicity. We propose an approximation, which expresses the equivalent impedance in a semi-analytical form. Full-wave simulations with ANSYS HFSS [24, 25] are performed in this work for several values of the ring radius and the wavenumber. The presented approach provides a useful design tool as it helps to carry out optimization and design without repeating the full-wave simulations, when the radius of the rings is changed.

The paper is organized as follows. Section 2 describes the equivalent circuit analysis without considering the substrate to illustrate the method in a simple way. Section 3 describes the equivalent circuit model but now including the substrate effects. Section 4 compares the results of the semi-analytical approach and measurements.

2. EQUIVALENT CIRCUIT ANALYSIS FOR CIRCULAR-RING ARRAY WITHOUT SUBSTRATE

2.1. Equivalent Circuit Model

The resonant behavior of the perfect electric conductor (PEC) periodic circular-ring structure can be described by a transmission line with a series circuit of a capacitance and an inductance, which is also used for Jerusalem-crosses and square loops [20, 21]. The effective impedance of these lumped elements depends on the geometric parameters of the circular ring and the periodicity. Figure 1 shows two identical unit-cells and the parameters of the circular ring: p is the periodicity (unit-cell length), r_{out} is the outer radius of the ring and r_{in} is the inner radius of the ring. The average radius is defined as

$$r_{av} = \frac{r_{in} + r_{out}}{2}. \tag{1}$$

In this study, we will use thin circular rings such that the values of r_{out} and r_{in} are assumed to be close to each other and the thickness of the rings to be negligible. The width of the rings are between 0.1 mm and 0.2 mm. Hence, the effective impedance of the lumped elements can be assumed to depend only on the average radius.

The effective impedance of the ring can be described by the reactance X in terms of a shunt inductive reactance X_L and a capacitive susceptance B_c as

$$X = X_L - \frac{1}{B_c}, \tag{2}$$

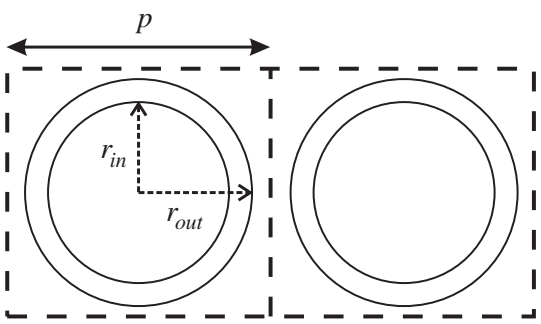

Figure 1. The unit-cells with circular rings in the middle.

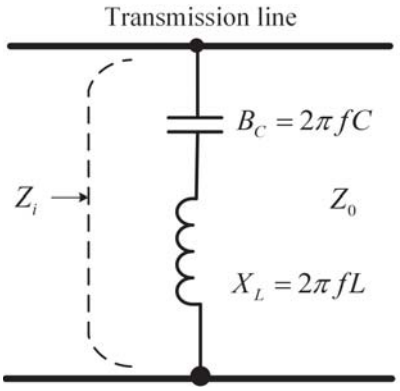

Figure 2. Equivalent circuit for planar circular metal rings.

where $X_L = 2\pi fL$, $B_c = 2\pi fC$ in Figure 2, f is the frequency, L the inductance, and C the capacitance. The reactance is normalized to the free space impedance Z_0 as

$$X_{nor} = \frac{2\pi fL}{Z_0} - \frac{1}{Z_0 2\pi fC} \tag{3}$$

and thus becomes unitless. In the following, we will always work with unitless quantities wherever possible to simplify calculations. The input impedance of the structure Z_i normalized to Z_0 is expressed through X_{nor} as [20]

$$Z_i = \frac{jX_{nor}}{jX_{nor} + 1}. \tag{4}$$

The transmission coefficient in terms of the impedance Z_i is given by

$$T = \frac{2Z_i}{Z_i + 1}. \tag{5}$$

The transmission coefficient is a complex number with real and imaginary parts in the form of

$$T = T_{real} + jT_{im}. \tag{6}$$

The real and imaginary parts of the transmission coefficient can be written in terms of the normalized reactance as

$$T_{real} = \frac{4X_{nor}^2}{1 + 4X_{nor}^2} \tag{7}$$

and

$$T_{im} = \frac{2X_{nor}}{1 + 4X_{nor}^2}. \tag{8}$$

In the following section, we will look for an expression for the inductance and capacitance of the array of circular rings.

2.2. Approximation for the Transmission Coefficient of an Array of Circular Rings

The transmission coefficient is assumed dependent on the average radius r_{av}, periodicity p, and free-space wavenumber $k = 2\pi f/c$, where c is the speed of light in free space. Since the transmission coefficient is dimensionless, it can be expressed in terms of two dimensionless parameters:

$$k_{nor} = kp \tag{9}$$

$$r_{nor} = \frac{r_{av}}{p}. \tag{10}$$

We rewrite expression (3) in terms of these parameters as

$$X_{nor} = k_{nor} F_1(r_{nor}) - \frac{1}{k_{nor}} F_2(r_{nor}), \tag{11}$$

where the coefficients F_1 and F_2 are unitless functions of r_{nor}.

For calculating the transmission coefficient, we insert Eq. (11) into Eqs. (7) and (8), which results in the following expressions:

$$T_{real}(r_{nor}, k_{nor}) = \frac{4(k_{nor}^2 F_1 - F_2)^2}{k_{nor}^2 + 4(k_{nor}^2 F_1 - F_2)^2} \tag{12}$$

$$T_{im}(r_{nor}, k_{nor}) = \frac{2k_{nor}^3 F_1 - 2k_{nor} F_2}{4k_{nor}^4 F_1^2 + k_{nor}^2(1 - 8F_1F_2) + 4F_2^2}. \tag{13}$$

The magnitude and phase of the transmission coefficient can be calculated as

$$|T| = \sqrt{T_{real}^2 + T_{im}^2} \tag{14}$$

$$\tan\theta_T = \frac{T_{im}}{T_{real}}. \tag{15}$$

Now we have an analytical expression for the complex transmission coefficient as a function of k_{nor} and r_{nor}. By analyzing this equation, we can find that a transmission blockage occurs when both the real and imaginary parts become zero, which leads to the condition

$$k_{nor}^2 = \frac{F_2}{F_1}. \tag{16}$$

Thus, the transmission blockage frequency depends only on the ratio of F_2 and F_1.

The transmission coefficient in Eqs. (12) and (13) depends only on the variable k_{nor} and the free parameters F_1 and F_2. In order to determine these free parameters, the absolute value of the transmission coefficient as given in Eq. (14) will be fitted to full-wave simulations for 7 different radii from 2.45 mm to 5.7 mm with one constant periodicity (12 mm). Figure 3 shows the amplitude of the transmission coefficient for the largest and the smallest values of r_{av} in the frequency range between 3 GHz and 30 GHz.

It should be pointed out that the free parameters F_1 and F_2 can also be determined by fitting

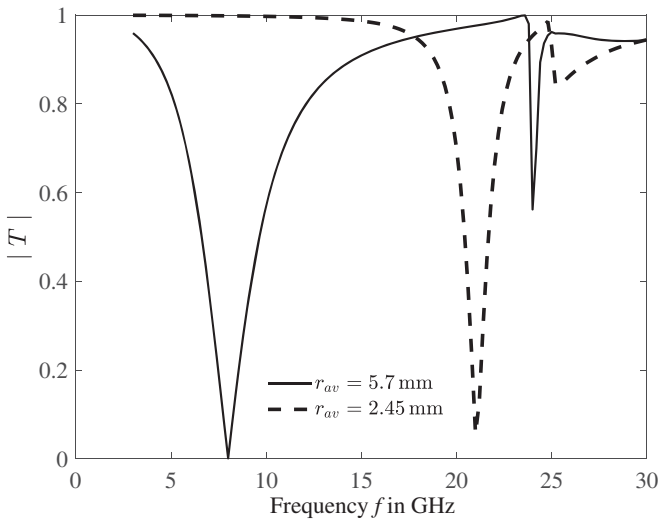

Figure 3. The full-wave simulated magnitude of the transmission coefficient of an array of circular rings without substrate for the largest and smallest radius values.

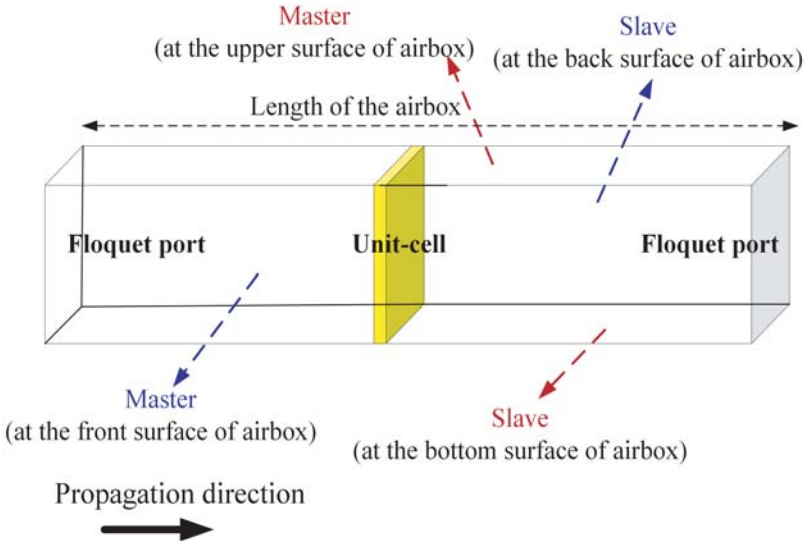

Figure 4. The setup used in HFSS simulations.

the phase of the transmission coefficient to the full-wave simulation results. Our test simulations have revealed however that both approaches seem to lead to close results. So, in this paper, only the magnitude value of the transmission coefficient is fitted. This approach is simple and sufficient as it gives the values of the free parameters, from which the real and imaginary parts and the phase of the transmission coefficient can be calculated by using Eqs. (12), (13) and (15).

Figure 4 shows the setup used in the full-wave simulations with ANSYS HFSS. The Floquet ports, which are used for excitation, are positioned as shown in Figure 4. The ring in the unit-cell (in Figure 4) is positioned in the middle of the airbox. The airbox between two Floquet ports has the length $\ell = 120\,\text{mm}$. To simulate the periodicity of the planar metamaterial array, master/slave boundary conditions, which are paired and applied on the surfaces with identical size and shape, are used [24, 25]. In order to extract the phase of the transmission coefficient, the simulation data for S_{21} is multiplied with $e^{jk\ell}$, which is the change in the phase of the incident wave traveling through the airbox. The material of airbox is vacuum.

Fitting Eq. (14) based on T_{real} and T_{im} given by Eqs. (12) and (13) in the Matlab curve fitting tool to the numerical data from full-wave simulations yields the values of F_1 and F_2 in Eqs. (12) and (13) for the selected 7 values of r_{nor} in Table 1. By fitting Eq. (17) to the data from Table 1, the coefficients a, b, c and d can be obtained as shown in Table 2. The curves plotted in Figure 5 show a good quality of

Table 1. Parameters F_1 and F_2 for several values of the average radius ($p = 12\,\text{mm}$).

r_{av} (mm)	2.45	2.7	3.5	3.9	4.45	4.9	5.7
F_1	0.9104	0.7232	0.5422	0.4872	0.5096	0.4134	0.3826
F_2	25.49	17.67	8.342	6.031	4.551	2.976	1.541

Table 2. Coefficients for exponential approximations in Eq. (17).

Coefficients	F_1	F_2
a	1347	1.015×10^5
b	−41.47	−46.32
c	0.9106	103.6
d	−1.826	−8.694

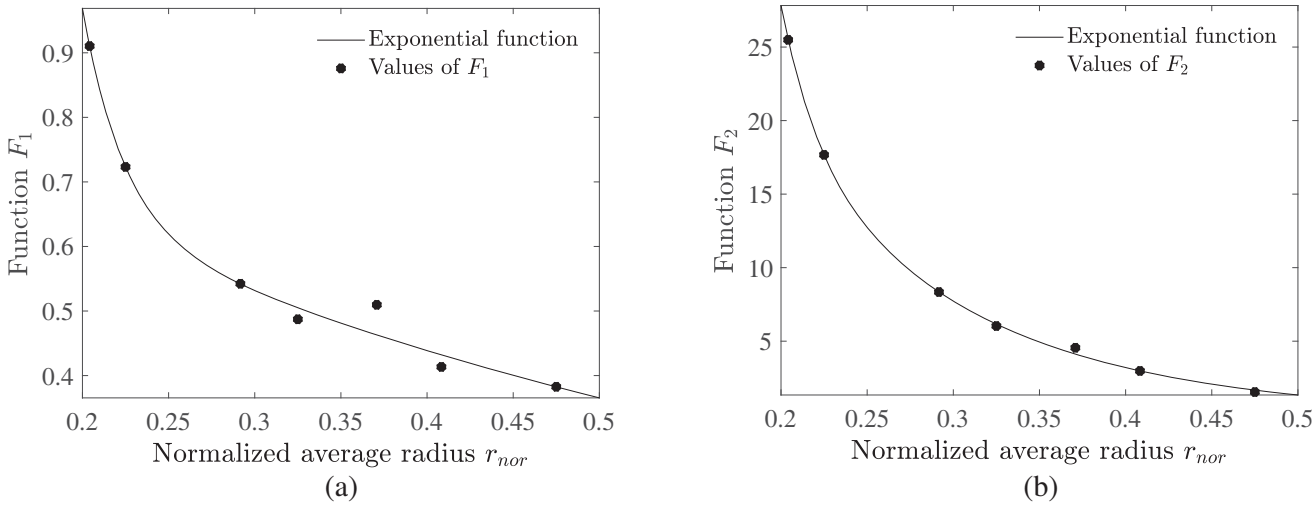

Figure 5. Exponential approximations obtained by fitting to the specific values of (a) F_1 and (b) F_2.

the approximation. The dependence of F_1 and F_2 on r_{nor} as shown in Figure 5 suggests the exponential approximations:

$$\begin{aligned} F_1(r_{nor}) &= a_1 e^{b_1 r_{nor}} + c_1 e^{d_1 r_{nor}} \\ F_2(r_{nor}) &= a_2 e^{b_2 r_{nor}} + c_2 e^{d_2 r_{nor}}. \end{aligned} \tag{17}$$

2.3. Comparison of Full-Wave Simulation and Semi-Analytical Approach

Let us compare the results of the semi-analytical approach with the results of the full-wave simulation for differently sized circular rings. We choose a radius value $r_{av} = 4.8\,\text{mm}$ from the interval $2.45\,\text{mm} \leq r_{av} \leq 5.7\,\text{mm}$ as in Table 1. In the simulation setup, the length of the airbox between the two Floquet ports for the simulation is 150 mm. As seen in Figure 6, there is a good match between the semi-analytical approach and the full-wave simulation.

The relation in Eq. (16) plays the main role for adjusting the blockage frequency. It follows from Eq. (16) that the value of k_{nor}, at which the transmission coefficient is at minimum, does not change if all geometrical dimensions of the structure are scaled with a proper factor. It is seen from Figure 7

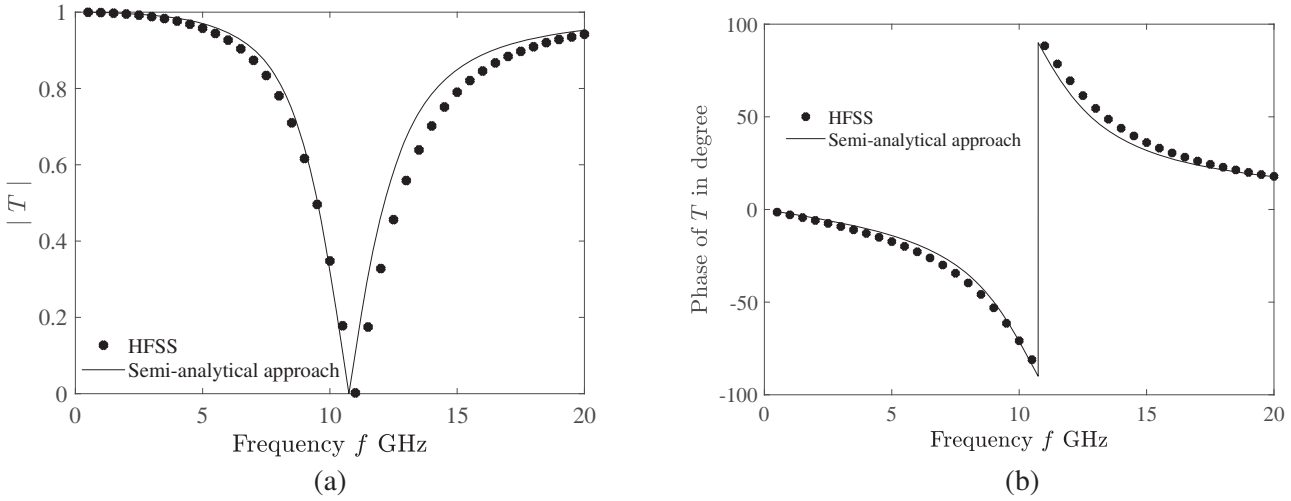

Figure 6. The transmission coefficient of an array of rings ($r_{out} = 4.9\,\text{mm}$, $r_{in} = 4.7\,\text{mm}$ and $p = 12\,\text{mm}$) without substrate. (a) Magnitude of the transmission coefficient. (b) Phase of the transmission coefficient.

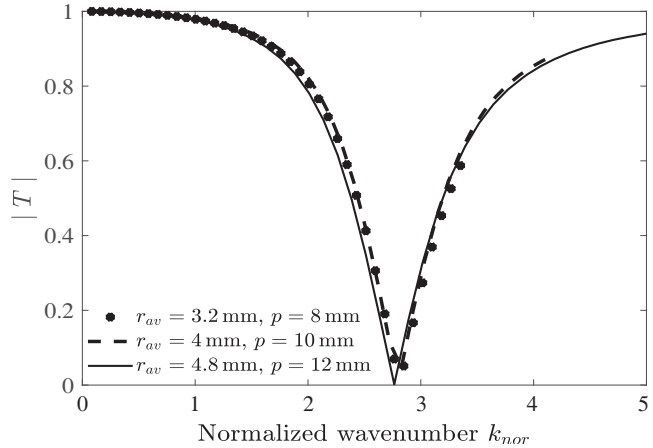

Figure 7. The magnitude of the full-wave simulated transmission coefficient of arrays of circular rings in free space with different values of r_{av} and p. The normalized radius is 0.4.

that the minima of the transmission coefficients for the arrays of the circular rings with three different radius values and periodicities are located almost at the same value of the normalized wavenumber ($k_{nor}^2 = 7.2942$), as expected.

As an intermediate conclusion, it can be said that the semi-analytical model for the arrays of PEC rings without substrate matches very well with full-wave simulation results.

3. EQUIVALENT CIRCUIT ANALYSIS FOR AN ARRAY OF CIRCULAR RINGS ON A DIELECTRIC SUBSTRATE

3.1. Analysis of Equivalent Circuit

A realistic metasheet is obtained by placing metal particles on a substrate as shown in Figure 8. In this section, a corresponding extension of the semi-analytical approximation is described. In the derivation, a layer of Rogers material RO3203 with the relative permittivity 3.02 and dielectric loss tangent 0.0016 is chosen as substrate. This low-loss and mechanically stable material is well suited for microwave applications [26, 27]. Even if we use this very specific material, the approach is generic and can be used for any dielectric substrate with or without losses.

The thickness of the substrate (ℓ_2) is chosen to be 3 mm. As in the previous section, we use thin metal rings whose width is between 0.1 mm and 0.2 mm, and the periodicity of the rings is 12 mm. The frequency range is between 0.5 GHz and 20 GHz. In this study, the losses are assumed to be small, so that the relative permittivity dominates.

For a lossy dielectric substrate the relative permittivity of the substrate and the dielectric tangent loss are given by

$$\begin{aligned} \varepsilon_r &= \varepsilon_r' - j\varepsilon_r'' \\ \tan\delta &= \frac{\varepsilon_r''}{\varepsilon_r'}. \end{aligned} \tag{18}$$

The value of the intrinsic impedance of the medium is

$$Z_d = \sqrt{\frac{\mu}{\varepsilon}} = \sqrt{\frac{\mu_0}{\varepsilon_r \varepsilon_0}} = \frac{Z_0}{\sqrt{\varepsilon_r}}. \tag{19}$$

The intrinsic impedance normalized to the free space impedance is given as

$$Z_{d,nor} = \frac{1}{\sqrt{\varepsilon_r' - j\varepsilon_r' \tan\delta}}. \tag{20}$$

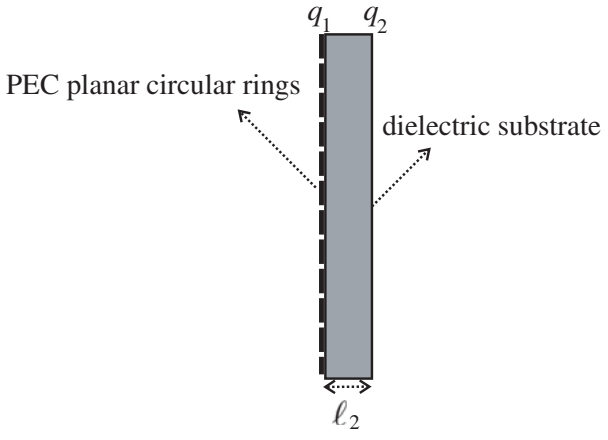

Figure 8. An array of planar circular rings on a dielectric substrate.

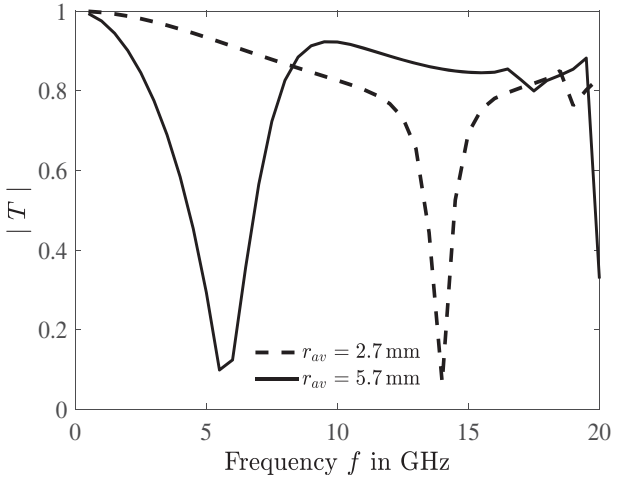

Figure 9. The full-wave simulated magnitude of the transmission coefficient of an array of circular rings on substrate RO3203 for the largest and smallest radius values.

The transmission coefficient for the structure in Figure 8 can be expressed as

$$T = \frac{(q_1+1)(q_2+1)e^{-k\ell_2(\alpha+j(\beta-1))}}{1+q_1q_2e^{-2k\ell_2(\alpha+j\beta)}}, \tag{21}$$

where $\alpha = \frac{\sqrt{\varepsilon_r'}\tan\delta}{2}$, and $\beta = \sqrt{\varepsilon_r'}$ [28, 29]. The parameters q_1 and q_2 are the internal reflection coefficients at the interfaces between the array of rings and the dielectric layer and between the dielectric layer and air [29],

$$q_1 = \frac{Z_i - Z_{d,nor}}{Z_i + Z_{d,nor}}, \tag{22}$$

$$q_2 = \frac{Z_{d,nor} - 1}{Z_{d,nor} + 1}. \tag{23}$$

The complex impedance Z_i is described in Eq. (4) with X_{nor} given by Eq. (11).

3.2. Approximation for the Transmission Coefficient of an Array of Circular Rings

Lumped elements of the same type as in Section 2.1 are used to describe the equivalent impedance Z_i of the infinite planar array of circular rings on the dielectric substrate. Full-wave simulations have been performed for 5 different radius values as shown in Table 3. Figure 9 shows the simulation results for the magnitude of the transmission coefficient for the largest (5.7 mm) and the smallest radius (2.7 mm) values.

Table 3. The results of curve fitting for arrays of circular rings on substrate RO3203.

r_{av} (mm)	F_1	F_2	$F_3 = \frac{F_2}{F_1}$
2.7	0.6958	8.546	12.2823
3.5	0.4683	3.617	7.7237
4.45	0.427	1.915	4.4848
4.9	0.3804	1.385	3.6409
5.7	0.3923	0.8109	2.0670

The same simulation setup as in Section 2.2 with the length of the airbox between Floquet ports equal to 150 mm has been used. The substrate in the unit-cell (in Figure 4) is positioned in the middle of the airbox, and the ring is adjusted on the substrate. Similar to Section 2.2, we fit the free parameters F_1 and F_2 in Eq. (11) to the full-wave simulation result for the amplitude of the transmission coefficient in Eq. (21). This yields the values for F_1 and F_2 as given in Table 3.

The substrate leads to a higher sensitivity of the blockage frequency with respect to the parameters F_1 and F_2. By analyzing Eq. (21), we see that the same relation as in Eq. (16) holds for the blockage frequency:

$$k_{nor}^2 = \frac{F_2}{F_1}. \tag{24}$$

Therefore, we introduce a new parameter F_3 which is defined by

$$F_3 = \frac{F_2}{F_1} \tag{25}$$

to make sure that the blockage frequency is approximated in the most accurate way. The dependency of F_1 and F_3 on r_{nor} is shown in Figure 10. A fitting process with the Matlab curve fitting tool yields the values of free coefficients a, b, c, and d as given in Table 4. F_2 can then be calculated from Eq. (25).

We use again exponential functions to describe this dependency:

$$\begin{aligned} F_1(r_{nor}) &= a_1e^{b_1r_{nor}} + c_1e^{d_1r_{nor}} \\ F_3(r_{nor}) &= a_3e^{b_3r_{nor}} + c_3e^{d_3r_{nor}}. \end{aligned} \tag{26}$$

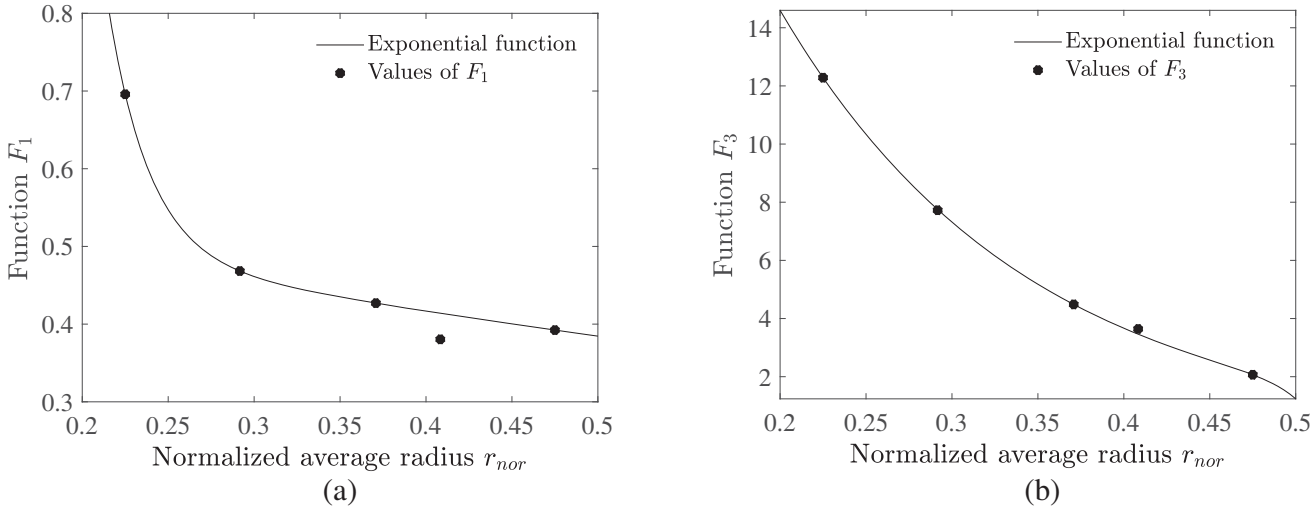

Figure 10. Exponential approximations obtained by fitting to the specific values of (a) F_1 and (b) F_3.

Table 4. Coefficients of the exponential approximations in Eq. (26).

Coefficients	F_1	F_3
a	2298	58.12
b	-41.2	-6.908
c	0.5742	-3.963×10^{-15}
d	-0.8019	65.3

By comparing the values of F_1 and F_2 in Tables 1 and 3, we see that the dielectric substrate mainly affects the capacitive part of the reactance (parameter F_2), which causes the change of the fundamental resonance frequency of the array of metal planar particles and the change of the bandwidth of the stopband region, which corresponds to what is reported in the literature, e.g., [30]. In our approach, the fitting should be repeated for different substrates and different thicknesses of the substrate.

3.3. Comparison of Full-Wave Simulations and Semi-Analytical Approach

To illustrate the accuracy of the semi-analytical approach, we have chosen two values of r_{av} from the range $2.7\,\text{mm} \leq r_{av} \leq 5.7\,\text{mm}$ which are different from the nodes used in the fitting procedure in Table 3. Figures 10 and 11 show a good approximation quality of the semi-analytical approximation.

It can also be clearly seen that even using copper instead of PEC for the rings gives well matching results in Figures 11 and 12.

4. COMPARISON WITH MEASUREMENTS

In this section we compare measurement results for two metasheets both based on the FR4 epoxy with two different copper ring sizes with our semi-analytical approach in Figures 13 and 14. FR4 is a cheaper material than RO3203 and thus used more frequently. It has a greater dissipation factor than many high-frequency laminates [31].

The same fitting process, explained in Section 3, is applied. The coefficients for the representations of F_1 and F_3 in Eq. (26) are calculated by matching the full-wave simulations at a selected set of values of r_{av}. The values of r_{av}, which are used in the fitting, are 2.7 mm, 3.5 mm, 4.45 mm, 4.9 mm and

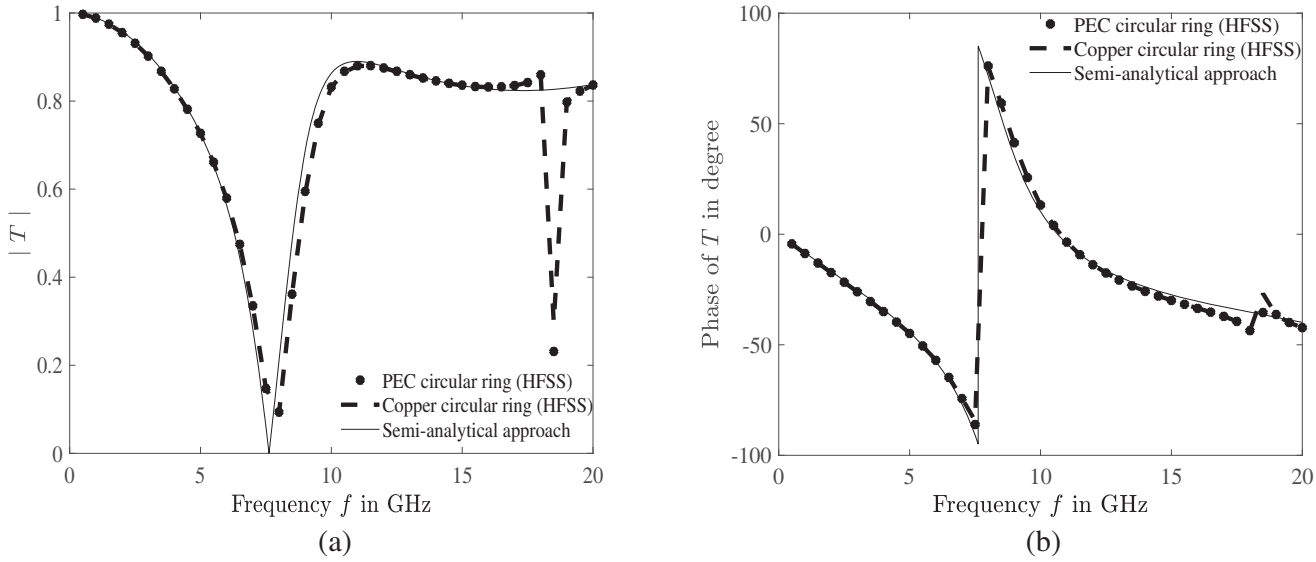

Figure 11. The transmission coefficient of an array of rings ($r_{out} = 4.9\,\text{mm}$, $r_{in} = 4.7\,\text{mm}$ and $p = 12\,\text{mm}$) on the dielectric substrate. (a) Magnitude of transmission coefficient. (b) Phase of transmission coefficient.

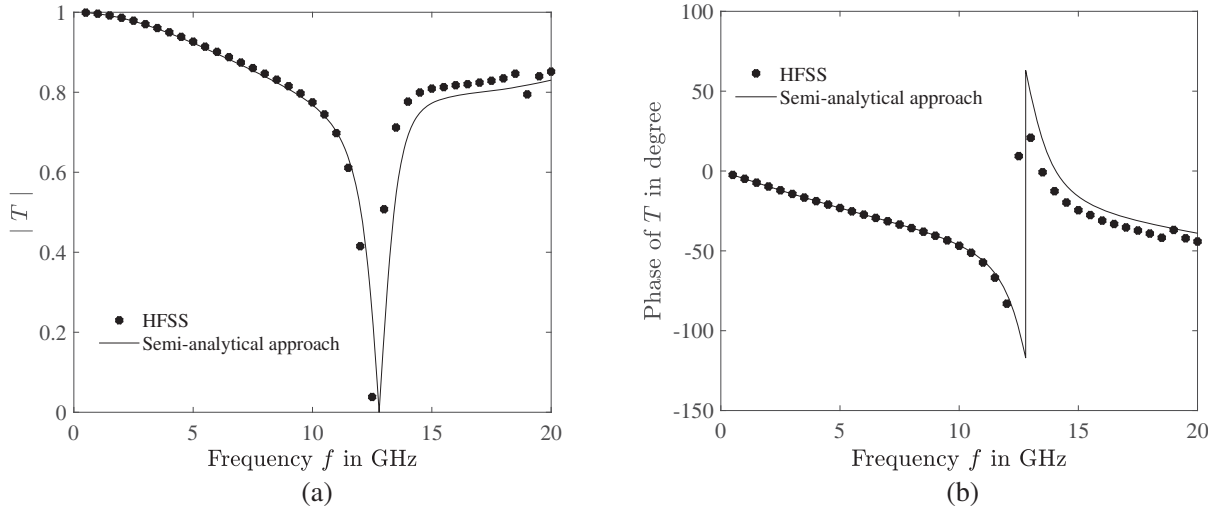

Figure 12. The transmission coefficient of an array of copper rings ($r_{out} = 3.05\,\text{mm}$, $r_{in} = 2.95\,\text{mm}$ and $p = 12\,\text{mm}$) on the dielectric substrate. (a) Magnitude of transmission coefficient. (b) Phase of transmission coefficient.

5.7 mm. The periodicity is 12 mm; the thickness of the substrate is 2 mm; the thickness of the ring is 0.018 mm. A normally incident plane wave is considered. Table 5 shows the obtained coefficients of the exponential function fitting.

The relative error in the blockage frequency can be estimated as

$$\text{Error} = \frac{|f_{\text{measurement}} - f_{\text{semi-analytical}}|}{f_{\text{measurement}}} \times 100\%. \tag{27}$$

With this the relative error for the ring with $r_{out} = 4.9\,\text{mm}$ and $r_{in} = 4.7\,\text{mm}$ is found to be 2.4%; for the ring with $r_{out} = 4.42\,\text{mm}$ and $r_{in} = 4.26\,\text{mm}$, the error equals 3.25%. We observe a very good match between the measurements and the semi-analytical approach as shown in Figures 13 and 14.

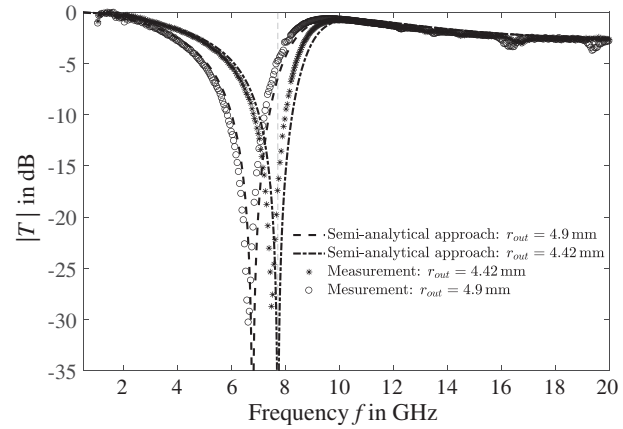

Figure 13. Comparison of results of semi-analytical approach and measurement for two arrays with differently sized rings: firstly $r_{out} = 4.9\,\text{mm}$, $r_{in} = 4.7\,\text{mm}$, secondly $r_{out} = 4.42\,\text{mm}$, $r_{in} = 4.26\,\text{mm}$.

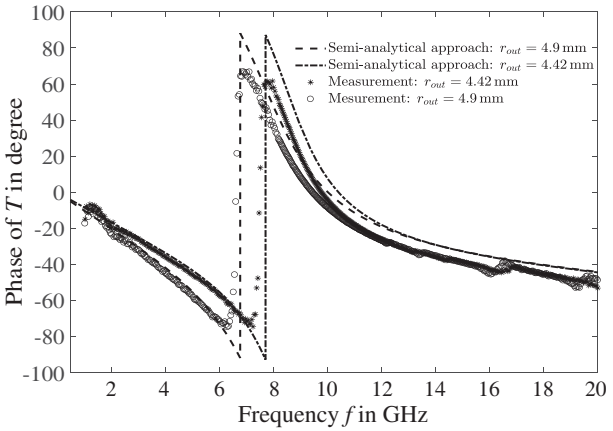

Figure 14. Comparison of results of semi-analytical approach and measurement for two arrays with differently sized rings: firstly $r_{out} = 4.9\,\text{mm}$, $r_{in} = 4.7\,\text{mm}$, secondly $r_{out} = 4.42\,\text{mm}$, $r_{in} = 4.26\,\text{mm}$.

Table 5. Coefficients of the exponential approximations in Eq. (26).

Coefficients	F_1	F_3
a	1.074	43.3
b	-2.383	-6.758
c	0	0
d	-150.5	-107.5

5. CONCLUSION

A semi-analytical approach, which is based on an equivalent circuit representation and parameter fitting, has been proposed for metasheets built from metal circular rings with and without dielectric substrate. The electromagnetic response of such metasheets can be controlled by simply changing the average radius of the rings and the periodicity of the array. The presented approach accelerates the metasheet design since it significantly reduces the number of required full-wave numerical simulations. In this paper a semi-analytical approach has been validated for two different dielectric substrates. The method can be extended to metasheets with other building elements.

REFERENCES

1. Öziş, E., A. Osipov, and T. F. Eibert, "Metamaterials for microwave radomes and the concept of a metaradome: Review of the literature," *International Journal of Antennas and Propagation*, Vol. 2017, No. 1356108, 1–13, 2017.
2. Michael, P. J. and P. M. Corcoran, "Asymmetric radome for phased antenna arrays," Patent US, No. 20100039346 A1, February 18, 2010.
3. Tretyakov, S. A., "Metasurfaces for general transformations of electromagnetic fields," *Philosophical Transactions of the Royal Society A: Mathematical, Physical and Engineering Sciences*, Vol. 373, No. 2049, 20140362, 2015.
4. Alù, A. and N. Engheta, "Enabling a new degree of wave control with metamaterials: A personal perspective," *Journal of Optics, Special Issue on History of Metamaterials*, Vol. 19, No. 084008, 1–10, 2017.

5. Bilotti, F., A. Toscano, L. Vegni, K. Aydin, K. B. Alici, and E. Özbay, "Equivalent-circuit models for the design of metamaterials based on artificial magnetic inclusions," *IEEE Transactions on Microwave Theory and Techniques*, Vol. 55, No. 12, 2865–2873, December 2007.
6. Zedler, M., C. Caloz, and P. Russer, "A 3-D isotropic left-handed metamaterial based on the rotated transmission-line matrix (TLM) scheme," *IEEE Transactions on Microwave Theory and Techniques*, Vol. 55, No. 12, 2930–2941, December 2007.
7. Zhu, B. O., K. Chen, N. Jia, L. Sun, J. Zhao, T. Jiang, and Y. Feng, "Dynamic control of electromagnetic wave propagation with the equivalent principle inspired tunable metasurface," *Scientific Reports*, Vol. 4, No. 4971, 1–7, May 2014.
8. Schelkunoff, S. A., "The impedance concept and its application to problems of reflection, refraction, shielding and power absorption," *The Bell System Technical Journal*, Vol. 17, No. 1, 17–48, 1938.
9. Schelkunoff, S. A., "Some equivalence theorems of electromagnetics and their application to radiation problems," *The Bell System Technical Journal*, Vol. 15, 92–112, 1936.
10. Labate, G., A. Alù, and L. Matekovits, "Surface admittance equivalence principle for non-radiating and cloaking problems," *Physical Review A*, Vol. 95, No. 063841, 1–7, 2017.
11. Volakis, J. L., T. F. Eibert, D. S. Filipovic, Y. E. Erdemli, and E. Topsakal, "Hybrid finite element methods for array and FSS analysis using multiresolution elements and fast integral techniques," *Electromagnetics*, Vol. 22, No. 4, 297–313, May 2002.
12. Eibert, T. F. and J. L. Volakis, "Adaptive integral method for hybrid FE/BI modelling of 3-D doubly periodic structures," *IEE Proceedings — Microwaves, Antennas and Propagation*, Vol. 146, No. 1, 17–22, February 1999.
13. Diest, K., L. A. Sweatlock, and D. E. Marthaler, "Metamaterials design using gradient-free numerical optimization," *Journal of Applied Physics*, Vol. 108, No. 084303, 1–5, 2010.
14. Paul, J., V. Podlozny, and C. Christopoulos, "The use of digital filtering techniques for the simulation of fine features in EMC problems solved in the time domain," *IEEE Transactions on Electromagnetic Compatibility*, Vol. 45, No. 2, 238–244, May 2003.
15. Christopoulos, C., *The Transmission-line Modeling Method (TLM)*, IEEE Press, New York, 1995.
16. Doncov, N., A. J. Wlodarczyk, R. Scaramuzza, and V. Trenkic, "Compact TLM for air-vents," *Electronics Letters*, Vol. 38, No. 16, 887–889, August 2002.
17. Holland, R. and L. Simpson, "Finite-difference analysis of EMP coupling to thin struts and wires," *IEEE Transactions on Electromagnetic Compatibility*, Vol. 23, 88–97, May 1981.
18. Duffy, A. P., et al., "New methods for accurate modelling of wires using TLM," *Electronic Letters*, Vol. 29, No. 2, 224–226, January 1993.
19. Trenkic, V., C. Christopoulos, and T. A. Benson, "Simple and elegant formulation of scattering in TLM nodes," *Electronics Letters*, Vol. 29, No. 18, 1651–1652, September 1993.
20. Anderson, I., "On the theory of self-resonant grids," *The Bell System Technical Journal*, Vol. 54, No. 10, 1725–1731, December 1975.
21. Langley, R. J. and E. A. Parker, "Equivalent circuit model for arrays of square loops," *Electronics Letters*, Vol. 18, No. 7, 294–296, 1982.
22. Munk, B. A., *Frequency Selective Surfaces: Theory and Design*, John Wiley and Sons, New York, 2000.
23. Labidi, M. and F. Choubani, "Electrical equivalent model of meta-materials based on circular SRR," *International Journal of Microwave and Wireless Technologies*, Vol. 8, No. 6, 909–913, September 2016.
24. Example-Endfire antenna array, Ansoft High Frequency Structure Simulator v11 User's Guide, [online], available: http://data.eefocus.com/myspace/33/165109/bbs/2010-01-04/1262563740_b4171 dec.pdf, [Accessed February 2018].
25. Workshop 9-1: Unit Cell Analysis (Infinite Array), Ansys, May 2015, [online], http://www.cadfamily.com/download-pdf/ANSYS-HFSS/ANSYS_HFSS_Antenna_W09_1_Unit _Cell.pdf, [Accessed 2018].

26. Rogers Corporation, [online], available: https://www.rogerscorp.com/acs/producttypes/6/RT-duroid-Laminates.aspx, [Accessed 2018].
27. Analyzing Advances in Antenna Materials, [online], available: http://www.rogerscorp.com /documents/1796/acm/articles/analyzing-advances-in-antenna-materials.pdf. [Accessed 2018].
28. Collin, R. E., *Foundations for Microwave Engineering*, Mc-Graw-Hill, 1992.
29. Orfanidis, S. J., *Electromagnetic Waves and Antennas*, http://www.ece.rutgers.edu/∼orfanidi/ewa/, [Accessed 2018], August 2016.
30. Callaghan, P., E. A. Parker, and R. J. Langley, "Influence of supporting dielectric layers on the transmission properties of frequency selective surfaces," *IEE Proceedings — H, Microwaves, Antennas and Propagation*, Vol. 138, No. 5, October 1991.
31. Coonrod, J., "Understanding when to use FR4 or high frequency laminates," *On Board Technology (www.Onboard-Technology.com)*, 26–30, September 2011.